Available online at www.sciencedirect.com
SCIENCE DIRECT
International Journal of Heat and Mass Transfer 49 (2006) 2502–2513
International Journal of HEAT and MASS TRANSFER
www.elsevier.com/locate/ijhmt

The effect of gaseous slip on microscale heat transfer: An extended Graetz problem

R.S. Myong [a,b,*], D.A. Lockerby [c], J.M. Reese [a]

[a] Department of Mechanical Engineering, University of Strathclyde, Glasgow G1 1XJ, United Kingdom
[b] Department of Mechanical and Aerospace Engineering and Research Center for Aircraft Parts Technology, Gyeongsang National University, Chinju, Kyeongnam 660-701, South Korea
[c] School of Engineering and Design, Brunel University, Uxbridge UB8 3PH, United Kingdom

Received 21 December 2004; received in revised form 11 October 2005
Available online 15 March 2006

Abstract

On the basis of Langmuir's theory of adsorption of gases on solids, the effect of temperature jump on microscale heat transfer is investigated. A mathematical model, extended from the classical Graetz problem, is developed to analyze convective heat transfer in a microtube in various slip-flow regimes. The surface slip corrections are made by employing the Langmuir model, as well as the conventional Maxwell model. The effects of axial heat conduction are also investigated by extending the finite integral transform technique to the slip-flow case. We show that the Langmuir model always predicts a reduction in heat transfer with increasing rarefaction, as does the Maxwell model, except when the energy accommodation coefficient is relatively much smaller than that for momentum accommodation. This implies that, for most physical applications, the Reynolds analogy between heat transfer and momentum transfer is preserved in slip-flow regimes with low Mach numbers.

Keywords: Extended Graetz problem; Temperature jump; Langmuir adsorption; Reynolds analogy; Microfluidics; Rarefied gas dynamics; Slip flow

1. Introduction

The study of non-linear transport in gas flows associated with micro and nanodevices [1,2] has emerged as an important topic in recent years. Understanding the fundamental physical phenomena [3–5] in such devices is essential in predicting their performance and searching for an optimal design. Several international theoretical and experimental research programmes are aiming to identify the main physical features of microscale gas flow and heat transfer [1,2,6]. The results of such fundamental work will be critical in answering questions about the usefulness of micro or nanodevices: can overall performance be improved by dividing a system into large numbers of microscale components? and can the traditional fluids knowledge base be applied in a scaled-down fashion to microfluidics?

In the field of microscale heat transfer, convective heat transfer in slip-flow regimes in simple geometries like channels and tubes is a key problem. Constant-wall-temperature convective heat transfer in microscale tubes and channels has been studied recently using analytical solutions to an extended Graetz problem [7–10] and DSMC simulations [10,11]. Using the fact that the characteristic speed in micro and nanodevices is usually very small (i.e. low Mach number), previous theoretical work has used the linear Navier–Stokes–Fourier equations (which rely on quasi local thermal equilibrium) to model flow and heat transfer phenomena. Accommodation coefficients of diffusive reflection were employed to describe the molecular interaction between the gas particles and solid surface atoms. The initial result in Ref. [7], based on the eigenvalues with velocity

* Corresponding author. Address: Department of Mechanical and Aerospace Engineering, Gyeongsang National University, Chinju, Kyeongnam 660-701, South Korea.
E-mail address: myong@nongae.gsnu.ac.kr (R.S. Myong).

0017-9310/$ - see front matter © 2006 Elsevier Ltd. All rights reserved.
doi:10.1016/j.ijheatmasstransfer.2005.11.035

Nomenclature

A_2	a coefficient depending on the exponent of the inverse power potential in Eq. (4)
$\mathscr{A}_{jn}$	coefficients defined in Eq. (66)
a	speed of sound
C	constant
C_c	concentration of the complex
C_m	concentration of the gas molecule
C_n	coefficients defined in Eq. (43)
C_s	concentration of the site
c_p	specific heat
D_e	potential parameter in the Langmuir slip model
F	eigenfunctions
$\mathscr{F}$	coefficients defined in Eq. (41)
${}_1F_1$	confluent hypergeometric function of the first kind (Kummer function)
h	heat transfer coefficient
K	equilibrium constant
k	Chapman–Enskog thermal conductivity
Kn	Knudsen number (l/L)
k_B	Boltzmann constant
L	characteristic length ($2R$)
l	mean free path
M	Mach number (U/a)
N	number of sites
$\mathscr{N}$	coefficient defined in Eq. (42)
m	molecular mass
N_δ	composite number ($\mu U_{ave}/(pL)$)
Nu	Nusselt number (Lh/k)
Pe	Peclet number ($Re \cdot Pr$)
Pr	Prandtl number ($\mu c_p/k$)
p	pressure
R	pipe radius
R_n	coefficients defined in Eq. (43)
Re	Reynolds number ($\rho U_{ave}(2R)/\mu$)
$\hat{r}$	dimensional radial coordinate
r	dimensionless radial coordinate ($\sqrt{\alpha}\hat{r}/R$)
T	temperature
T_m	bulk-average temperature
T_w	wall temperature
T_0	inlet temperature
U	gas velocity
U_{ave}	gas flux-average velocity ($U_{ave} = U_{max}(2-\alpha)/2$)
U_{max}	gas maximum velocity (at the tube centerline)
u	dimensionless gas velocity (U/U_{max})
x	a variable
$\hat{z}$	axial coordinate
z	dimensionless axial coordinate ($\hat{z}\alpha(2-\alpha)/(RPe)$)
z^+	dimensionless axial coordinate ($\hat{z}/(RPe)$)

Greek symbols

α	fraction of surface covered at equilibrium
$\sqrt{\alpha}$	slip radius
β	a parameter in the Langmuir slip model ($K/(k_B T)$)
$\bar{\beta}$	a coefficient in the Langmuir slip model ($1/(4\omega Kn)$)
γ	specific heat ratio
Γ	gamma function
Δ_n	coefficients defined in Eq. (61)
θ	dimensionless temperature ($(T-T_w)/(T_0-T_w)$)
$\tilde{\theta}$	a component of the dimensionless temperature ($\theta(r,z) = \tilde{\theta}(r,z) + \theta_0\theta(0,z)$)
θ_0	downstream limit of the dimensionless temperature (θ_0=$1-\alpha$)
θ_m	dimensionless bulk-average temperature
Θ_j	transformed variables of the temperature $\tilde{\theta}$
λ_n	eigenvalue
Λ_n	coefficients defined in Eqs. (57), (68) and (79)
μ	Chapman–Enskog viscosity
ν	exponent of the inverse power laws
ρ	density
$\bar{\sigma}$	ratio of energy accommodation to momentum accommodation (σ_T/σ_v)
σ_v	a coefficient of momentum accommodation $[(2-\phi_v)/\phi_v]$
σ_T	a coefficient of energy accommodation $[(2-\phi_T)/\phi_T \cdot 2\gamma/(\gamma+1)\cdot 1/Pr]$
ϕ_v	momentum accommodation coefficient
ϕ_T	thermal accommodation coefficient
ω	an accommodation coefficient in the Langmuir slip model defined in Eq. (4)
ω_0	coefficient in the Langmuir slip model defined in Eq. (4)

Subscripts

r	reference condition
n,j	n,jth eigenvalue

slip only [12], indicated that heat transfer increases as the degree of rarefaction increases. This seemed doubtful, physically, as the famous experimental observations of Millikan [13] indicated that the drag coefficient decreases with increasing rarefaction. As a result, the so-called Reynolds analogy between heat transfer and momentum transfer was not preserved in this previous work [7]. At the same time, a careful investigation [8] in which the temperature slip is taken into account revealed a more complicated picture: that heat transfer can increase or decrease with increasing rarefaction, depending on the ratio of energy accommodation to momentum accommodation. Even though this result is very instructive in its own right, a conceptual problem remains. The core result depends on the

ratio of two free parameters (the accommodation coefficients) which must be chosen by other means, for example, from experimental data.

Recently some new developments have been reported on modelling gaseous slip phenomena from the viewpoint of the gas-surface molecular interaction [14–18]. This may provide useful information which could help solve the aforementioned problem. An important result obtained from this work is that a physical slip model can be derived from Langmuir's theory of gaseous adsorption on solids (gas molecules can be adsorbed onto a surface owing to long range forces between the gas particles and the surface atoms). As a result, it has been shown that a physical meaning (heat adsorption) can be assigned to the accommodation coefficient in the Maxwell model; otherwise it is a free parameter to be determined by other means. It is therefore interesting to examine whether the Reynolds analogy is preserved in this Langmuir model.

The objective of our present work is to investigate microscale heat transfer where the gaseous slips at the solid surface, in particular the temperature jump, are the dominant phenomena. Slip corrections will be made by employing the new Langmuir model as well as the conventional Maxwell model. Our emphasis will be on the qualitative features of microscale heat transfer, for example, enhancement or reduction of heat transfer in microscale geometries. For the purpose of avoiding numerical uncertainty in these low-speed gas flows, we adopt an analytical solution approach and all our calculations are done with the help of a high-accuracy numerical program.

2. Temperature slip based on Langmuir adsorption

2.1. Langmuir's slip model

A physical approach to describing the slip can be developed by taking into account the interfacial interaction between the gas molecules and the surface molecules. In this approach the gas molecules are assumed to interact with the surface of the solid via a long range attractive force. Consequently the gas molecules can be adsorbed onto the surface, and then desorbed after some time lag. This mechanism of the deposition of a layer with a thickness of one or more molecules onto the surface is known as adsorption in the literature of surface chemistry [19,20]. If we model this interaction as a chemical reaction in which the gas molecule, m, and the site, s, form the complex, c, we may obtain an expression for the fraction of the surface covered by adsorbed atoms at thermal equilibrium, α:

$$\alpha = (1-\alpha)\beta p \quad \text{or} \quad \alpha = \frac{\beta p}{1+\beta p}, \quad \text{where}$$

$$\beta = \frac{K}{k_B T_w} \quad \text{and} \quad K = \frac{C_c}{C_m C_s}. \tag{1}$$

The fraction α is a function of the pressure, p, and the equilibrium constant, K, which are functions of the concentrations $C_{m,s,c}$, and the surface temperature, T_w. As the pressure increases, its value approaches unity, implying that most of the molecules are at thermal equilibrium.

With information about the fraction of the surface covered at equilibrium determined by this Langmuir adsorption isotherm, it is possible to develop a slip model for the gas-surface molecular interaction. The velocity and temperature slip can be expressed, in dimensional form, as [14–16]

$$u = \alpha u_w + (1-\alpha)u_g, \qquad T = \alpha T_w + (1-\alpha)T_g, \tag{2}$$

where subscript g denotes a local value adjacent to the wall, for example, a mean free path away from the wall, or a reference value such as the free-stream condition. The only parameter requiring further investigation is β (or the equilibrium constant K). A previous study [16] showed that the parameter β takes the form

$$\beta = \frac{1}{4\omega Kn}\frac{1}{p_r}, \tag{3}$$

where

$$\omega = \omega_0(v)\left(\frac{T_w}{T_r}\right)^{1+2/(v-1)} \exp\left(-\frac{D_e}{k_B T_w}\right),$$

$$\omega_0(v) = \frac{8\sqrt{2}}{5\pi} A_2(v)\Gamma\left[4-\frac{2}{v-1}\right]. \tag{4}$$

Then Eq. (1) reduces to (in dimensionless form),

$$\alpha = \frac{\bar{\beta}p}{1+\bar{\beta}p}, \quad \text{where} \quad \bar{\beta} = \frac{1}{4\omega Kn}. \tag{5}$$

Tabulated values of $A_2(v)$ and $\omega_0(v)$ are given in Table 1 for exponents $v > 2$ [3,21]. The coefficient ω_0 has a value between 1.02806 (for $v = 6$) and 1.52001 (for $v = 3$) and becomes 1.44051 (for $v \to \infty$) for rigid elastic sphere molecules. The role of the coefficient ω, which is a function of v, T_w, and D_e, is very similar to the slip coefficient, σ, in the Maxwell model. For most molecular interaction models,

Table 1
Tabulated values of $A_2(v)$ and $\omega_0(v)$ for an inverse power-law molecular force

v	$A_2(v)$	$\omega_0(v)$
3	1.05519	1.52001
4	0.56081	1.12217
5	0.43619	1.04409
6	0.38401	1.02807
7	0.35675	1.03094
8	0.34066	1.04056
9	0.33040	1.05255
10	0.32352	1.06517
11	0.31873	1.07762
12	0.31530	1.08955
13	0.31282	1.10090
14	0.31099	1.11157
15	0.30964	1.12160
20	0.30674	1.16325
50	0.31113	1.27766
∞	0.33333	1.44051

the value of the heat of adsorption, D_e, falls within the range $O(10^{-1}$–10) kcal/mol. Its value may be inferred from theoretical predictions of intermolecular forces, or from experimental data.

A few comments should be added with regard to the characteristics of this slip model, and their implications. First, in the present model there are no terms related to high-order effects, such as thermal creep and viscous heat dissipation. This is in contrast to the common practice of including them in the original formulation but later ignoring them by assuming a low Mach number flow. The same spirit is taken in the development of our model, but it is implemented differently. The composite number, N_δ, defined as the ratio of viscous forces to the hydrostatic pressure, is a parameter which indicates the degree of thermal non-equilibrium in macroscopic thermodynamic space. It can be shown that the nature of the constitutive equations in either the moment method [5] or the Chapman–Enskog method [3] depends primarily on this parameter. Consequently, the slip phenomenon consists largely of two components: one being the non-Newtonian effect in the bulk flow region measured by the composite number, N_δ, and the other being the gas-surface molecular interaction measured by the Knudsen number, Kn. The former is of purely hydrodynamic origin, and has nothing to do with the gas-surface molecular interaction. It is responsible for non-linear coupling effects, including the aforementioned high-order effects. Since $N_\delta \approx Kn \cdot M$, these non-linear effects are usually negligible for small Mach number, meaning that the linear Navier–Stokes–Fourier equations can still be valid in most low-speed microscale gas flows. However, coupling between the normal and shear stresses may be non-negligible even when N_δ is small, and this may produce a Knudsen-layer effect even at low speeds. While this remains to be investigated, in any case, it is of lesser importance than the slip effect due to the gas-surface molecular interaction and consequently it is ignored in our present study. Non-negligible Knudsen numbers in microscale gas flows require some kind of model capable of describing the slip phenomenon.

The second comment we make here is that, within this new framework, there is no distinction between momentum and energy accommodation: they are represented by a single parameter α ($0 \leqslant \alpha \leqslant 1$), the fraction of the surface covered by adsorbed atoms at thermal equilibrium. This feature is in some sense equivalent to the case of equal momentum and energy accommodation in the Maxwell model. Since the ratio of momentum and energy accommodation plays a crucial role in determining the qualitative features of microscale heat transfer, enhancing or reducing heat transfer [7,8,10,22], this difference may have important implications. This will be discussed in detail in Section 3. However, when we consider the fact that the accommodation coefficients in the Maxwell model do not depend explicitly on the wall temperature, while the parameter α in the Langmuir model is a function of the wall temperature, the difference is largely related to how one implements the wall temperature dependence. Therefore, it can be said that there is no prior theoretical justification in favor of one model or the other, except that the Langmuir model is simpler (involving only one parameter, instead of two in the case of the Maxwell model).

2.2. The extended Graetz problem

The low-speed microscale (creeping) regime, typical of gas flows in microsystems at atmospheric conditions, generally falls within the non-equilibrium parameter ranges

$$Kn = O(10^{-2}\text{–}1), \qquad N_\delta = O(10^{-5}\text{–}10^{-2}).$$

In this range of small values of N_δ, the Newtonian (Navier–Stokes–Fourier) constitutive equations are assumed to be valid. On the other hand, non-negligible Knudsen numbers require a slip model for the gas-surface molecular interaction. If we consider monatomic gas flow and heat transfer in forced laminar flow through a circular tube with constant-wall temperature with the usual assumptions of the classical Graetz problem, i.e. fully developed flow, incompressible, constant-properties gas, and high Peclet number [23], the momentum and energy equations may be expressed as

$$\frac{1}{\hat{r}}\frac{\mathrm{d}}{\mathrm{d}\hat{r}}\left(\hat{r}\frac{\mathrm{d}U}{\mathrm{d}\hat{r}}\right) = C, \tag{6}$$

$$\rho c_p U \frac{\partial T}{\partial \hat{z}} = k\frac{1}{\hat{r}}\frac{\partial}{\partial \hat{r}}\left(\hat{r}\frac{\partial T}{\partial \hat{r}}\right), \tag{7}$$

with the Langmuir slip boundary conditions at the stationary wall

$$U(\hat{r} = R) = (1-\alpha)U_{\max}, \tag{8}$$

$$T(\hat{r} = R, \hat{z}) = \alpha T_{\mathrm{w}} + (1-\alpha)T(\hat{r} = 0, \hat{z}), \tag{9}$$

where the non-equilibrium parameter α is related to $\bar{\beta}$ by the relation

$$\alpha = \frac{\bar{\beta}}{1+\bar{\beta}} \tag{10}$$

and other boundary conditions of

$$\left[\frac{\partial U}{\partial \hat{r}}\right]_{\hat{r}=0} = 0, \tag{11}$$

$$\left[\frac{\partial T}{\partial \hat{r}}\right]_{\hat{r}=0} = 0, \tag{12}$$

$$T(\hat{r}, \hat{z} = 0) = T_0. \tag{13}$$

In the temperature jump boundary condition (9), a local temperature at the tube centerline $T(\hat{r} = 0, \hat{z})$ is used as the reference temperature T_g so as to take into account the axial variation of the gas temperature adjacent to the tube wall. This is in the same spirit as the Maxwell model, where such variation is included through the radial gradient of local temperature near the wall.

It is worth mentioning that our present model can be easily extended to treat flow in a microchannel with a minor change accounting for the different geometry [9,10].

If we calculate the velocity profile $U(\hat{r})$ by solving (6) with the boundary conditions (8) and (11), we obtain the following solution:

$$U(\hat{r}) = \frac{C}{4}(\hat{r}^2 - R^2) + (1-\alpha)U_{\max}, \tag{14}$$

where C is a constant. As $U_{\max}$ represents the gas velocity at the tube centerline, the dimensionless velocity can then be written as

$$\frac{U(\hat{r})}{U_{\max}} = 1 - \alpha\frac{\hat{r}^2}{R^2}. \tag{15}$$

With a dimensionless variable defined through

$$r = \sqrt{\alpha}\frac{\hat{r}}{R}, \tag{16}$$

Eq. (15) reduces to

$$u(r) = 1 - r^2. \tag{17}$$

Here, the parameter $\sqrt{\alpha}$ represents a slip radius, which was first introduced by Larrodé et al. [8] in the context of the Maxwell slip model. After inserting the velocity solution into the energy equation and introducing the following dimensionless variables and relations

$$\theta = \frac{T - T_w}{T_0 - T_w}, \quad z = \frac{\hat{z}}{R}\frac{\alpha(2-\alpha)}{Pe}, \tag{18}$$

$$U_{ave} = U_{\max}\frac{(2-\alpha)}{2}, \quad Re = \frac{\rho U_{ave}(2R)}{\mu}, \quad Pr = \frac{\mu c_p}{k},$$

$$Pe = Pr \cdot Re, \tag{19}$$

we obtain the following equations for the temperature profile

$$(1-r^2)\frac{\partial\theta}{\partial z} = \frac{1}{r}\frac{\partial}{\partial r}\left(r\frac{\partial\theta}{\partial r}\right) \tag{20}$$

and boundary conditions

$$\theta(r = \sqrt{\alpha}, z) = \theta_0\theta(r = 0, z), \tag{21}$$

$$\left[\frac{\partial\theta}{\partial r}\right]_{r=0} = 0, \tag{22}$$

$$\theta(r, z = 0) = 1, \tag{23}$$

where

$$\theta_0 = 1 - \alpha.$$

In the limit of continuum gas flow (i.e. $Kn \to 0$, $\bar{\beta} \to \infty$, $\alpha \to 1$) the usual dimensionless variables are recovered and the problem reduces to the classical Graetz problem, which can be solved analytically using orthogonal eigenfunctions of the Sturm–Liouville boundary value problem [24,25]. On the other hand, the value of θ at the wall becomes non-zero in slip flow and consequently the mathematical problem involves non-homogeneous boundary conditions. However, if we note that the governing equation is linear, and that the coordinate z plays a role very similar to the time, we may solve it by reducing it to a problem with homogeneous boundary conditions. Specifically, via the assumption of

$$\theta(r, z) = \tilde{\theta}(r, z) + \theta_0\theta(r = 0, z) \tag{24}$$

and

$$\tilde{\theta}(r = 0, z) = (1 - \theta_0)\theta(r = 0, z) \tag{25}$$

the problem reduces to

$$(1-r^2)\left[\frac{\partial\tilde{\theta}}{\partial z} + \frac{\theta_0}{1-\theta_0}\frac{d\tilde{\theta}(r=0,z)}{dz}\right] = \frac{1}{r}\frac{\partial}{\partial r}\left(r\frac{\partial\tilde{\theta}}{\partial r}\right), \tag{26}$$

with boundary conditions

$$\tilde{\theta}(r = \sqrt{\alpha}, z) = 0, \tag{27}$$

$$\left[\frac{\partial\tilde{\theta}}{\partial r}\right]_{r=0} = 0, \tag{28}$$

$$\tilde{\theta}(r, z = 0) = 1 - \theta_0. \tag{29}$$

The mathematical problem of the temperature distribution $\tilde{\theta}(r, z)$ is no longer a type of classical Sturm–Liouville boundary value problem, owing to the second term on the lefthand side of the differential equation (26). However, it is still possible to develop an approximate method by which the qualitative aspect of the slip effect in microscale heat transfer can be obtained. If the term, $\frac{\theta_0}{1-\theta_0}\frac{d\tilde{\theta}(r=0,z)}{dz}$, is ignored it is straightforward to obtain an exact solution, since the equation for the transient temperature distribution $\tilde{\theta}(r, z)$ is then exactly the same as in the classical Graetz problem, except for a different constant value at the inlet condition and the wall boundary condition at $r = \sqrt{\alpha}$ instead of $r = 1$

$$\tilde{\theta}(r, z) = \sum_{n=1}^{\infty} a_n \exp\left(-\lambda_n^2 z\right)F_n(r), \tag{30}$$

where the eigenfunctions $F_n(r)$ satisfy

$$\frac{d}{dr}\left(r\frac{dF}{dr}\right) + \lambda_n^2 w(r)F = 0, \tag{31}$$

subject to the homogeneous boundary conditions

$$F(r = \sqrt{\alpha}) = 0, \tag{32}$$

$$\left[\frac{dF}{dr}\right]_{r=0} = 0. \tag{33}$$

Here the weighting function $w(r)$ is defined as

$$w(r) = r(1 - r^2)$$

and $w(r) \geqslant 0$ at all points in $0 \leqslant r \leqslant \sqrt{\alpha}$. The eigenfunctions may be expressed in terms of the confluent hypergeometric function of the first kind ${}_1F_1$ as follows (with the normalization $F(0) = 1$)

$$F_n(r) = \exp\left(-\frac{\lambda_n}{2}r^2\right){}_1F_1\left[\frac{1}{2} - \frac{\lambda_n}{4}; 1; \lambda_n r^2\right]. \tag{34}$$

It should be mentioned that due to the ill-posedness at $r = 0$ the confluent hypergeometric function of the second

kind [26,27] is excluded from the solution. The function ${}_1F_1$, also known as the Kummer function in the literature [27,28], is defined as an infinite series

$$ {}_1F_1(a;b;x) = 1 + \frac{a}{b}x + \frac{a(a+1)}{b(b+1)}\frac{x^2}{2!} + \frac{a(a+1)(a+2)}{b(b+1)(b+2)}\frac{x^3}{3!} + \cdots \tag{35} $$

and satisfies the following relation:

$$ \frac{\mathrm{d}}{\mathrm{d}x}\left[{}_1F_1(a;b;x)\right] = \frac{a}{b}\,{}_1F_1(a+1;b+1;x). \tag{36} $$

Then the eigenvalues λ_n can be obtained by solving the transcendental equation that arises from applying boundary condition (32) to the function (34)

$$ {}_1F_1\left[\frac{1}{2} - \frac{\lambda_n}{4}; 1; \lambda_n\alpha\right] = 0. \tag{37} $$

For further analysis, a first-order approximation to the nth positive zero of the function ${}_1F_1(a;b;x)$ for large $\frac{1}{2}b - a$ [27,29] is also given as

$$ x_n \doteq \frac{\pi^2\left(n + \frac{1}{2}b - \frac{3}{4}\right)^2}{2b - 4a}. \tag{38} $$

The constants a_n can be determined from the boundary condition (29) by utilizing the orthogonality properties of the eigenfunctions

$$ a_n = \alpha\frac{\mathscr{F}_n}{\mathscr{N}_n}, \tag{39} $$

which can be further simplified into

$$ a_n = \alpha(-)\frac{4\sqrt{\alpha}}{C_n\lambda_n} \tag{40} $$

by invoking the following useful relations

$$ \begin{aligned} \mathscr{F}_n &\equiv \int_0^{\sqrt{\alpha}} w(r)F_n(r)\mathrm{d}r \\ &= -\frac{\sqrt{\alpha}R_n}{\lambda_n^2}\left[= \left(-\frac{1}{\lambda_n^2}\right)\int_0^{\sqrt{\alpha}}\frac{\mathrm{d}}{\mathrm{d}r}\left(r\frac{\mathrm{d}F}{\mathrm{d}r}\right)\mathrm{d}r\right], \end{aligned} \tag{41} $$

$$ \begin{aligned} \mathscr{N}_n &\equiv \int_0^{\sqrt{\alpha}} w(r)F_n^2(r)\mathrm{d}r \\ &= \frac{C_nR_n}{4\lambda_n}\left[= \frac{\sqrt{\alpha}}{2\lambda_n}\left[\frac{\partial F_n}{\partial\lambda}\frac{\partial F_n}{\partial r} - F_n\frac{\partial^2 F_n}{\partial\lambda\partial r}\right]_{r=\sqrt{\alpha}}\right], \end{aligned} \tag{42} $$

where the coefficients R_n and C_n are defined by

$$ R_n = \left[\frac{\partial F_n}{\partial r}\right]_{r=\sqrt{\alpha}}, \quad C_n = 2\sqrt{\alpha}\left[\frac{\partial F_n}{\partial\lambda}\right]_{r=\sqrt{\alpha}}. \tag{43} $$

In deriving relation (42) L'Hospital's rule was used. Finally the local temperature distribution can be described as

$$ \tilde{\theta}(r,z) = \alpha(-4\sqrt{\alpha})\sum_{n=1}^{\infty}\frac{\exp\left(-\lambda_n^2 z\right)F_n(r)}{C_n\lambda_n}. \tag{44} $$

Then the flux-averaged mean temperature

$$ \tilde{\theta}_{\mathrm{m}}(z) = \frac{\int_0^{\sqrt{\alpha}}\tilde{\theta}(r,z)w(r)\mathrm{d}r}{\int_0^{\sqrt{\alpha}}w(r)\mathrm{d}r}, \tag{45} $$

reduces to

$$ \tilde{\theta}_{\mathrm{m}}(z) = \frac{16\alpha}{2-\alpha}\sum_{n=1}^{\infty}\frac{R_n\exp(-\lambda_n^2 z)}{C_n\lambda_n^3}. \tag{46} $$

In addition, the Nusselt number, defined as

$$ Nu = \frac{(-2R)}{T_{\mathrm{m}} - T_{\mathrm{w}}}\left[\frac{\partial T}{\partial r}\right]_{r=R} = \frac{(-2\sqrt{\alpha})}{\tilde{\theta}_{\mathrm{m}}}\left[\frac{\partial\tilde{\theta}}{\partial r}\right]_{r=\sqrt{\alpha}}, \tag{47} $$

becomes

$$ Nu = \frac{\alpha(2-\alpha)}{2}\frac{\sum_{n=1}^{\infty}R_n\exp(-\lambda_n^2 z)/(C_n\lambda_n)}{\sum_{n=1}^{\infty}R_n\exp(-\lambda_n^2 z)/(C_n\lambda_n^3)}. \tag{48} $$

It can be easily verified that the solution of the classical Graetz problem is recovered in the continuum limit $\alpha \to 1$.

From these results, an approximate solution of the non-classical Sturm–Liouville boundary value problem can be constructed by considering an auxiliary problem of orthogonal eigenfunctions $F_n(r)$ associated with the Graetz problem, which are given in Eqs. (31)–(33) and (37). Here we will extend a finite integral transform technique [30,31] to solve an extended Graetz problem in the slip-flow case. It is straightforward to identify the following integral transform pair from this problem:

$$ \text{Transform}: \Theta_j(z) = \int_0^{\sqrt{\alpha}} w(r)F_j(r)\tilde{\theta}(r,z)\mathrm{d}r, \tag{49} $$

$$ \text{Inversion}: \tilde{\theta}(r,z) = \sum_{j=1}^{\infty}\frac{1}{\mathscr{N}_j}F_j(r)\Theta_j(z). \tag{50} $$

If we apply an operation $\int_0^{\sqrt{\alpha}} rF_j(r)\mathrm{d}r$ to Eq. (26) and note that

$$ \frac{\mathrm{d}\tilde{\theta}(r=0,z)}{\mathrm{d}z} = \sum_{j=1}^{\infty}\frac{1}{\mathscr{N}_j}\frac{\mathrm{d}\Theta_j(z)}{\mathrm{d}z}, \tag{51} $$

then we have

$$ \frac{\mathrm{d}\Theta_j(z)}{\mathrm{d}z} + \frac{\theta_0\mathscr{F}_j}{1-\theta_0}\sum_{n=1}^{\infty}\frac{1}{\mathscr{N}_n}\frac{\mathrm{d}\Theta_n(z)}{\mathrm{d}z} = -\lambda_j^2\Theta_j(z), \quad j = 1,2,\ldots. \tag{52} $$

The transformed form of the boundary condition (29) can be written as

$$ \Theta_j(z=0) = (1-\theta_0)\mathscr{F}_j. \tag{53} $$

The system (52) is an infinite set of coupled first-order differential equations for the transforms $\Theta_j(z)$. Once they are determined, the transient temperature distribution $\tilde{\theta}(r,z)$ can be obtained by the inversion formula. Here we are interested only in qualitative aspects of the effects of the temperature jump, so we limit ourselves to the explicit

lowest order solution. By retaining only one term in the series ($j = n$), we obtain the following decoupled system:

$$\left(1+\frac{\theta_0}{1-\theta_0}\frac{\mathscr{F}_n}{\mathscr{N}_n}\right)\frac{\mathrm{d}\Theta_n}{\mathrm{d}z}+\lambda_n^2\Theta_n=0 \quad n=1,2,\ldots \tag{54}$$

with

$$\Theta_n(z=0)=(1-\theta_0)\mathscr{F}_n. \tag{55}$$

The solutions are

$$\Theta_n(z)=(1-\theta_0)\mathscr{F}_n\exp(-\Lambda_n^2 z), \tag{56}$$

where

$$\Lambda_n^2=\frac{\lambda_n^2}{1+\dfrac{\theta_0}{1-\theta_0}\dfrac{\mathscr{F}_n}{\mathscr{N}_n}}=\frac{\lambda_n^2}{1-\dfrac{\theta_0}{1-\theta_0}\dfrac{4\sqrt{\alpha}}{C_n\lambda_n}}. \tag{57}$$

Then the temperature distribution can be given approximately as

$$\theta(r,z)=-4\sqrt{\alpha}\sum_{n=1}^{\infty}\frac{\exp(-\Lambda_n^2 z)}{C_n\lambda_n}[(1-\theta_0)F_n(r)+\theta_0]. \tag{58}$$

Other important equations follow:

$$\theta_{\mathrm{m}}(z)=\frac{16(1-\theta_0)}{2-\alpha}\sum_{n=1}^{\infty}\frac{R_n\exp(-\Lambda_n^2 z)}{C_n\lambda_n^3}[1+\theta_0\Delta_n], \tag{59}$$

$$Nu=\frac{\alpha(2-\alpha)}{2}\frac{\sum_{n=1}^{\infty}R_n\exp(-\Lambda_n^2 z)/(C_n\lambda_n)}{\sum_{n=1}^{\infty}[1+\theta_0\Delta_n]R_n\exp(-\Lambda_n^2 z)/(C_n\lambda_n^3)}, \tag{60}$$

where

$$\Delta_n\equiv-\frac{\sqrt{\alpha}(2-\alpha)}{4(1-\theta_0)R_n}\lambda_n^2. \tag{61}$$

2.3. The effect of axial heat conduction

An implicit assumption made in the Graetz problem is that of a high Peclet number ($Pe = Re\cdot Pr$), meaning that the axial conduction is negligible in comparison with the axial convection. Inclusion of the effects of axial heat conduction may, however, be necessary in microscale heat transfer since the Peclet number in small-scale geometries is usually low.

If we include the axial conduction term in the energy equation, the resulting equation can be expressed in dimensionless form as

$$(1-r^2)\frac{\partial\theta}{\partial z}=\frac{1}{r}\frac{\partial}{\partial r}\left(r\frac{\partial\theta}{\partial r}\right)+\frac{1}{\overline{Pe}^2}\frac{\partial^2\theta}{\partial z^2}, \tag{62}$$

where

$$\overline{Pe}=\frac{Pe}{\sqrt{\alpha}(2-\alpha)}. \tag{63}$$

Then the new problem is equivalent to solving

$$(1-r^2)\left[\frac{\partial\tilde{\theta}}{\partial z}+\frac{\theta_0}{1-\theta_0}\frac{\mathrm{d}\tilde{\theta}(r=0,z)}{\mathrm{d}z}\right]=\frac{1}{r}\frac{\partial}{\partial r}\left(r\frac{\partial\tilde{\theta}}{\partial r}\right)+\frac{1}{\overline{Pe}^2}\frac{\partial^2\tilde{\theta}}{\partial z^2}, \tag{64}$$

with the same boundary conditions as in Eqs. (27)–(29).

In order to treat the effect of axial heat conduction, various approaches have been developed in the literature; for example, expanding the temperature field in terms of the infinite Fourier sine series [32,33] or expressing the non-orthogonal eigenfunctions in terms of the eigenfunction of an auxiliary orthogonal system [34]. Here we again use a finite integral transform technique [30,31] to handle the second order term. The transformed form of the governing Eq. (64) reduces to

$$\frac{\mathrm{d}\Theta_j(z)}{\mathrm{d}z}+\frac{\theta_0\mathscr{F}_j}{1-\theta_0}\sum_{n=1}^{\infty}\frac{1}{\mathscr{N}_n}\frac{\mathrm{d}\Theta_n(z)}{\mathrm{d}z}=-\lambda_j^2\Theta_j(z)+\frac{1}{\overline{Pe}^2}\sum_{n=1}^{\infty}\mathscr{A}_{jn}\frac{\mathrm{d}^2\Theta_n(z)}{\mathrm{d}z^2}, \quad j=1,2,\ldots, \tag{65}$$

where

$$\mathscr{A}_{jn}=\frac{1}{\mathscr{N}_n}\int_0^{\sqrt{\alpha}}rF_j(r)F_n(r)\mathrm{d}r. \tag{66}$$

By retaining only one term in the series ($j = n$), we obtain the following second order decoupled system:

$$\frac{\mathscr{A}_{nn}}{\overline{Pe}^2}\frac{\mathrm{d}^2\Theta_n}{\mathrm{d}z^2}-\left(1+\frac{\theta_0}{1-\theta_0}\frac{\mathscr{F}_n}{\mathscr{N}_n}\right)\frac{\mathrm{d}\Theta_n}{\mathrm{d}z}-\lambda_n^2\Theta_n=0, \quad n=1,2,\ldots \tag{67}$$

For this differential equation we have the following coefficients

$$\Lambda_n^2=\frac{1}{2}\frac{\overline{Pe}^2}{\mathscr{A}_{nn}}\times\frac{\left[\left(1-\frac{\theta_0}{1-\theta_0}\frac{4\sqrt{\alpha}}{C_n\lambda_n}\right)^2+4\lambda_n^2\frac{\mathscr{A}_{nn}}{\overline{Pe}^2}\left(1-\frac{\theta_0}{1-\theta_0}\frac{4\sqrt{\alpha}}{C_n\lambda_n\mathscr{A}_{nn}}\right)\right]^{1/2}-\left(1-\frac{\theta_0}{1-\theta_0}\frac{4\sqrt{\alpha}}{C_n\lambda_n}\right)}{1-\frac{\theta_0}{1-\theta_0}\frac{4\sqrt{\alpha}}{C_n\lambda_n\mathscr{A}_{nn}}}. \tag{68}$$

It can be noted that the effect of axial conduction appears only through the term Λ_n; in other words, the solution of the case involving axial conduction can be obtained simply by replacing Eq. (57).

2.4. Comparison with Maxwell's slip model

An alternative way of including slip is to make a correction based on the degree of non-equilibrium near the wall surface, which can best be represented by the shear stress and heat flux. This idea can be traced to the work of Maxwell [35] and subsequent work by Smoluchowski [36] in which the following slip boundary conditions are proposed:

$$U(\hat{r}=R)=\sigma_{\mathrm{v}} l\left[-\frac{\mathrm{d}U}{\mathrm{d}\hat{r}}\right]_{\hat{r}=R}, \tag{69}$$

$$T(\hat{r}=R)=T_{\mathrm{w}}+\sigma_{\mathrm{T}} l\left[-\frac{\mathrm{d}T}{\mathrm{d}\hat{r}}\right]_{\hat{r}=R}, \tag{70}$$

where l is the gas molecular mean free path. It is also possible to include non-linear coupling effects like thermal creep and viscous heat dissipation, but they are assumed to be negligible in the present study under the assumption of small Mach number.

In principle, the coefficients σ_{v} and σ_{T} may depend on various properties of the interaction of the gas with the surface: the gas and surface temperatures, the surface roughness, the type of gas molecules (i.e. monatomic or diatomic) and type of surface molecules. However, these dependences are neglected in most models and they are usually incorporated into overall accommodation coefficients which express the degree of diffusive reflection at the surface

$$\sigma_{\mathrm{v}}=\frac{2-\phi_{\mathrm{v}}}{\phi_{\mathrm{v}}}, \tag{71}$$

$$\sigma_{\mathrm{T}}=\frac{2-\phi_{\mathrm{T}}}{\phi_{\mathrm{T}}}\frac{2\gamma}{\gamma+1}\frac{1}{Pr}, \tag{72}$$

where ϕ_{v} and ϕ_{T} represent momentum and thermal accommodation coefficients. In practice, their values are chosen so that they fit best to the experimental data and are tabulated for various gases and surfaces.

We now apply the Maxwell slip conditions (69) and (70) to the momentum and energy Eqs. (6) and (7). It is straightforward to show that, with a definition

$$\alpha=\frac{1}{1+4\sigma_{\mathrm{v}} Kn}, \tag{73}$$

the resulting velocity profile is exactly the same as the one in the Langmuir slip model (17). In addition, if the following relation is assumed,

$$\sigma_{\mathrm{v}}=\omega, \tag{74}$$

the slip radius in the Maxwell slip model becomes equivalent to that ($\sqrt{\alpha}$) in the Langmuir slip model.

On the other hand, there do exist differences in the results for the temperature distribution, which can be identified by examining the solutions of the Graetz problem with the Maxwell slip boundary conditions derived by Larrodé et al. [8]. Specifically, by using the mixed boundary condition of the Maxwell slip model (70) in place of the non-homogeneous boundary condition of the Langmuir slip model (21) we can derive a different series solution to the Sturm–Liouville boundary value problem:

$$\theta(r,z)=\sum_{n=1}^{\infty} a_n \exp(-\lambda_n^2 z)F_n(r), \tag{75}$$

with a homogeneous (mixed) boundary condition

$$F(r=\sqrt{\alpha})+\frac{\bar{\sigma}}{2}\frac{(1-\alpha)}{\sqrt{\alpha}}\left[\frac{\mathrm{d}F}{\mathrm{d}r}\right]_{r=\sqrt{\alpha}}=0, \tag{76}$$

where $\bar{\sigma}$ represents the ratio of energy accommodation to momentum accommodation,

$$\bar{\sigma}=\frac{\sigma_{\mathrm{T}}}{\sigma_{\mathrm{v}}}.$$

Because of the mixed boundary condition the transcendental equation takes the following complicated form:

$${}_1F_1\left[\frac{1}{2}-\frac{\lambda_n}{4};1;\lambda_n\alpha\right]+\frac{\bar{\sigma}}{2}\lambda_n(1-\alpha),$$
$$\left(\frac{2-\lambda_n}{2}{}_1F_1\left[\frac{3}{2}-\frac{\lambda_n}{4};2;\lambda_n\alpha\right]-{}_1F_1\left[\frac{1}{2}-\frac{\lambda_n}{4};1;\lambda_n\alpha\right]\right)=0. \tag{77}$$

Other important relations remain the same as in Eqs. (44), (46) and (48). Similar to the previous case, the solution reduces to the classical Graetz solution in the continuum limit. A more detailed derivation may be found in Ref. [8].

A similar technique can be applied to the case involving axial heat conduction. By using the transformed form of the Maxwell boundary condition, we have

$$\Theta_n(z=0)=\mathscr{F}_n. \tag{78}$$

Due to the second order term the new eigenvalues become

$$\Lambda_n^2=\frac{1}{2}\frac{\overline{Pe}^2}{\mathscr{A}_{nn}}\left[\left(1+4\lambda_n^2\frac{\mathscr{A}_{nn}}{\overline{Pe}^2}\right)^{1/2}-1\right]. \tag{79}$$

Then we obtain the following results (where the effect of axial conduction appears through the term Λ_n):

$$\theta(r,z)=-4\sqrt{\alpha}\sum_{n=1}^{\infty}\frac{\exp(-\Lambda_n^2 z)F_n(r)}{C_n\lambda_n}, \tag{80}$$

$$\theta_{\mathrm{m}}(z)=\frac{16}{2-\alpha}\sum_{n=1}^{\infty}\frac{R_n\exp(-\Lambda_n^2 z)}{C_n\lambda_n^3}, \tag{81}$$

$$Nu=\frac{\alpha(2-\alpha)}{2}\frac{\sum_{n=1}^{\infty}R_n\exp(-\Lambda_n^2 z)/(C_n\lambda_n)}{\sum_{n=1}^{\infty}R_n\exp(-\Lambda_n^2 z)/(C_n\lambda_n^3)}. \tag{82}$$

3. Results and discussion

The numerical evaluation of the local temperature distribution and the Nusselt number for a given value of α requires information about the eigenvalues λ_n and the coefficients R_n, C_n and $\mathscr{A}_{nn}$. The eigenvalues can be calculated from Eq. (37) using a root-finding method (for example, the secant method). Once the eigenvalues are known, the eigenfunctions can be determined from Eq. (34). Then the coefficients R_n, C_n and $\mathscr{A}_{nn}$ can be obtained by evaluating the integrals (41), (42) and (66) numerically. We perform all these calculations with the help of the high-accuracy numerical program *Mathematica* [37]. However, accurate asymptotic expressions similar to the one developed for the original Graetz series in Ref. [38] may be needed when a detailed knowledge of the temperature distribution near the entrance is required. Similarly, we evaluate the eigenvalues λ_n in the Maxwell model by solving the

transcendental Eq. (77) using *Mathematica* [12,37]. The numerical values of the eigenvalues and coefficients in the Langmuir model are summarized for different Knudsen numbers (0.0–0.12) in Table 2. The first seven eigenvalues and coefficients were obtained from an exact evaluation. Since we are interested mainly in the qualitative aspects of the slip models, only a case with non-negligible Knudsen number (0.02) is considered for the Maxwell model, and this is summarized in Table 3.

The effect of rarefaction, represented by α, on the eigenvalues λ_n and coefficients R_n, C_n and $\mathscr{A}_{nn}$ is shown in Table 2. It can be seen that there is a monotonic variation in the eigenvalues λ_n and coefficients $\mathscr{A}_{nn}$. In fact, the increase in magnitude of the eigenvalues with increasing rarefaction can be predicted by an approximate relation $\lambda_n \approx \pi(n-\frac{1}{4})/\sqrt{\alpha}$, which may be derived by combining Eqs. (37) and (38). On the other hand, the trend is reversed in the case of the Maxwell model, which can be observed from Table 3. The perturbrative calculation of the eigenvalues for Eq. (77) [8] indicates that the first-order correction depends on the parameter $(1-\bar{\sigma})$ and consequently it is negative for the present case with $\bar{\sigma} = 15/8$. It should be mentioned, however, that the difference in the effect of rarefaction on the eigenvalues has no physical importance and is related to different mathematical forms of the slip models: one of the Dirichlet type and the other of the Neumann type.

Fig. 1 shows the effect of rarefaction on the local Nusselt number along the tube using the Langmuir model. It is assumed that the axial conduction is small in comparison

Table 2
Eigenvalues λ_n and other coefficients ($R_n, C_n, \mathscr{A}_{nn}$) in the Langmuir slip model for different Knudsen numbers ($\omega = 1.0$)

$Kn\backslash\lambda_n$	λ_1	λ_2	λ_3	λ_4	λ_5	λ_6	λ_7
(a)							
0.00	2.70436	6.67903	10.6734	14.6711	18.6699	22.6691	26.6687
0.005	2.72456	6.71548	10.7232	14.7329	18.7427	22.7523	26.7616
0.02	2.78455	6.82612	10.8773	14.9270	18.9748	23.0209	27.0658
0.04	2.86309	6.97560	11.0909	15.2017	19.3090	23.4137	27.5165
0.06	2.93999	7.12611	11.3103	15.4883	19.6622	23.8331	28.0019
0.08	3.01530	7.27672	11.5330	15.7824	20.0273	24.2692	28.5091
0.10	3.08906	7.42678	11.7573	16.0806	20.3994	24.7154	29.0295
0.12	3.16133	7.57587	11.9820	16.3808	20.7753	25.1671	29.5572
$Kn\backslash R_n$	R_1	R_2	R_3	R_4	R_5	R_6	R_7
(b)							
0.00	−1.01430	1.34924	−1.57233	1.74602	−1.89088	2.01643	−2.12820
0.005	−1.02953	1.37849	−1.61518	1.80228	−1.96034	2.09904	−2.22369
0.02	−1.07394	1.46243	−1.73654	1.95963	−2.15265	2.32535	−2.48329
0.04	−1.13052	1.56656	−1.88394	2.14720	−2.37798	2.58646	−2.77841
0.06	−1.18443	1.66326	−2.01793	2.31467	−2.57605	2.81278	−3.03100
0.08	−1.23602	1.75380	−2.14122	2.46664	−2.75363	3.01360	−3.25320
0.10	−1.28555	1.83915	−2.25584	2.60636	−2.91547	3.19535	−3.45309
0.12	−1.33326	1.92008	−2.36332	2.73627	−3.06498	3.36238	−3.63605
$Kn\backslash C_n$	C_1	C_2	C_3	C_4	C_5	C_6	C_7
(c)							
0.00	−1.001800	0.742925	−0.636523	0.572959	−0.528975	0.495998	−0.469928
0.005	−0.982258	0.724541	−0.617701	0.553493	−0.508876	0.475282	−0.448671
0.02	−0.928106	0.675197	−0.568652	0.504164	−0.459160	0.425213	−0.398283
0.04	−0.864818	0.620159	−0.516226	0.453380	−0.409679	0.376861	−0.350968
0.06	−0.809814	0.574288	−0.474128	0.413851	−0.372168	0.341046	−0.316627
0.08	−0.761523	0.535306	−0.439310	0.381849	−0.342341	0.312986	−0.290052
0.10	−0.718764	0.501664	−0.409858	0.355200	−0.317797	0.290115	−0.268558
0.12	−0.680621	0.472266	−0.384510	0.332519	−0.297081	0.270935	−0.250623
$Kn\backslash\mathscr{A}_{nn}$	$\mathscr{A}_{11}$	$\mathscr{A}_{22}$	$\mathscr{A}_{33}$	$\mathscr{A}_{44}$	$\mathscr{A}_{55}$	$\mathscr{A}_{66}$	$\mathscr{A}_{77}$
(d)							
0.00	1.25123	1.45617	1.53713	1.58458	1.61707	1.64133	1.66037
0.005	1.24570	1.44449	1.52187	1.56664	1.59699	1.61940	1.63687
0.02	1.23045	1.41241	1.48010	1.51779	1.54245	1.56009	1.57340
0.04	1.21279	1.37564	1.43268	1.46286	1.48171	1.49461	1.50397
0.06	1.19761	1.34448	1.39306	1.41756	1.43220	1.44185	1.44861
0.08	1.18442	1.31782	1.35967	1.37985	1.39147	1.39888	1.40392
0.10	1.17286	1.29481	1.33124	1.34813	1.35755	1.36338	1.36725
0.12	1.16265	1.27478	1.30681	1.32115	1.32892	1.33363	1.33669

Table 3
Eigenvalues λ_n and other coefficients ($R_n, C_n, \mathscr{A}_{nn}$) in the Maxwell slip model ($Kn = 0.02$, $\sigma_v = 1.0, \bar{\sigma} = 15/8$)

n	λ_n	R_n	C_n	$\mathscr{A}_{nn}$
1	2.63250	−1.03304	−1.000140	1.27146
2	6.55378	1.33356	0.760266	1.49615
3	10.5081	−1.51051	−0.668529	1.58485
4	14.4737	1.63120	0.617769	1.63486
5	18.4462	−1.71800	−0.585686	1.66686
6	22.4239	1.78166	0.564091	1.68856
7	26.4060	−1.82849	−0.549087	1.70363

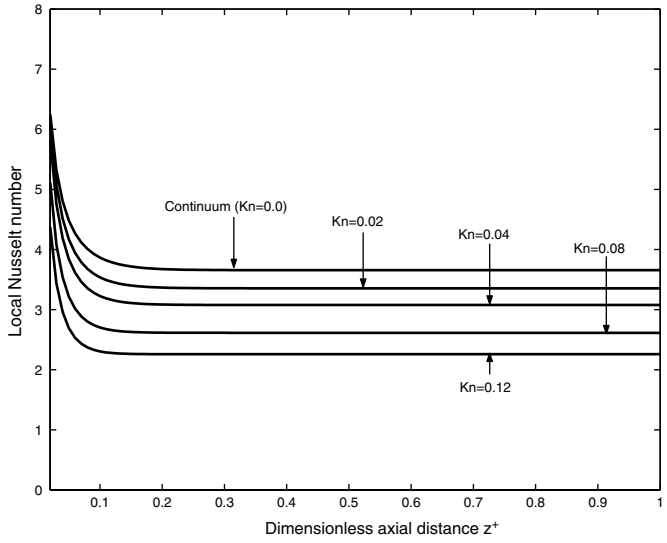

Fig. 1. Local Nusselt number along the tube for different values of Kn (equivalently, α) ($\omega = 1.0$, $P_e = 10.0$).

with the axial convection ($Pe = 10.0$). It can be seen that the heat transfer, represented by the Nusselt number, always decreases with increasing rarefaction. Therefore the Reynolds analogy is preserved in the case of the Langmuir model.

In passing, it would be of interest to check the accuracy of the present approximate solution. A simple error estimate is possible by substituting the lowest order solution Eq. (56) into the coupled differential equation (52). (The case without axial conduction is considered for simplicity.) The determinant of a matrix in which non-diagonal terms were neglected in the lowest order solution, $\alpha^2 \Lambda_1^2 \Lambda_2^2 \mathscr{F}_1^2 \mathscr{F}_2^2 \exp[-(\Lambda_1^2 + \Lambda_2^2)z]/(\mathscr{N}_1 \mathscr{N}_2)$ when the first two eigenvalues are considered, can serve as an error estimate. This reduces to $1.485\exp(-56.55z^+)$ ($\mathscr{F}_1 = 0.1333$, $\mathscr{F}_2 = -0.0302$), and at $z^+ = 0.05$ its value becomes 0.0879. This analysis indicates that the present solution is very close to the exact solution, especially for large values of z^+.

In order to examine the effect of the Peclet number on the variation of the local Nusselt number, two cases ($Pe = 10.0, Pe \to \infty$) are illustrated in Fig. 2. This figure indicates that the effect of axial heat conduction is to increase the local Nusselt number along the tube. As the

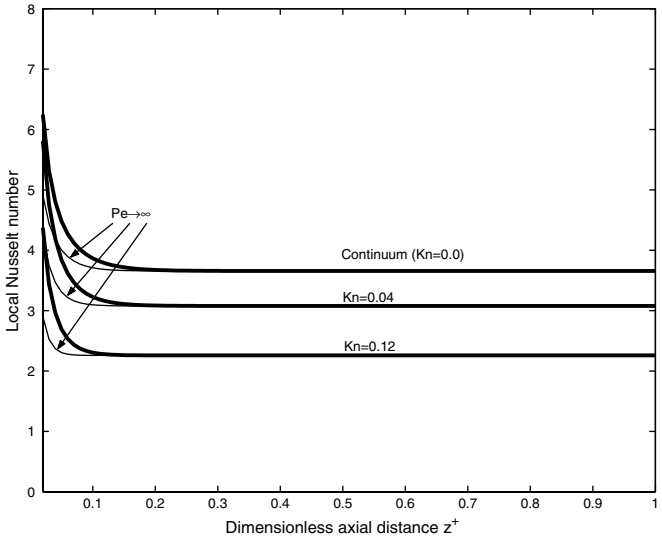

Fig. 2. Effect of axial heat conduction on the variation of Nusselt number. The thin solid lines denote the solutions without axial heat conduction ($Pe \to \infty$) while the thick solid lines represent the solutions with axial heat conduction ($Pe = 10.0$).

Peclet number decreases, Eq. (68) reduces to $\Lambda_1 < \lambda_1$ and therefore the local Nusselt number in Eq. (60) increases. It can also be seen in the figure that the effect of axial heat conduction decreases with increasing rarefaction. That is, as the value of α decreases with increasing rarefaction, the value of $\overline{Pe}^2/\mathscr{A}_{11}$ increases and as a result $\Lambda_1 \to \lambda_1$. Thus the increment in the local Nusselt number by axial heat conduction is reduced for increasing rarefaction. These qualitative properties are, in fact, in agreement with the independent result of Ref. [10], where both an analytical method using the Maxwell model and DSMC simulations are employed.

Fig. 3 shows a comparison of the local Nusselt numbers along the tube predicted by the Maxwell model. The

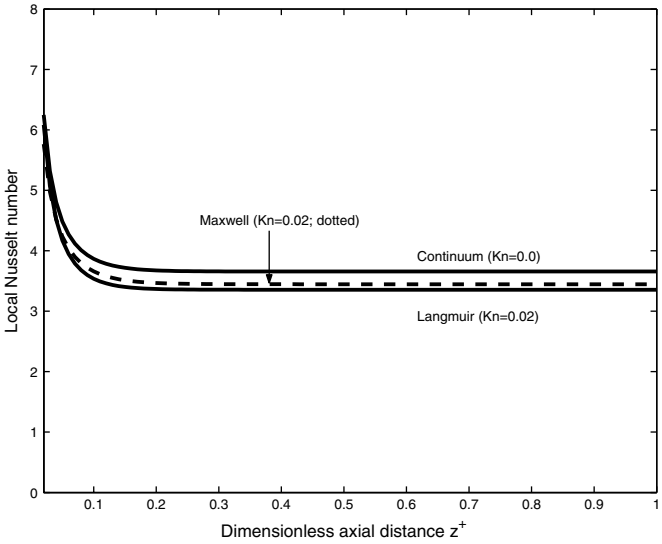

Fig. 3. Comparison of local Nusselt number along the tube using the Maxwell model ($Kn = 0.02$, $Pe = 10.0, \gamma = \frac{5}{3}$, $Pr = \frac{2}{3}$, $\bar{\sigma} = 15/8$).

assumption of equal momentum and energy accommodation coefficients $\phi_v = \phi_T$, or $\bar{\sigma} = 15/8$, for $\gamma = \frac{5}{3}$ and $Pr = \frac{2}{3}$ is used here. This figure shows that heat transfer reduces with increasing rarefaction in both models, even though the level of reduction is slightly more pronounced in the Langmuir models. This finding coincides with the conclusion of Ref. [8] that a heat transfer reduction is predicted for $\bar{\sigma} > 1$ in slip flow. Note also from Fig. 3 that there exists an asymptotic value of the Nusselt number in both the Maxwell and Langmuir models. (In comparison, $Nu \approx 3.657$ for the continuum case, 3.446 in the Maxwell model and 3.355 in the Langmuir model, for $Kn = 0.02$.)

Fig. 4 shows the axial variation of temperature, measured at the centerline of the tube, $\theta(r = 0, z^+)$, for Knudsen numbers (0.0, 0.02). The eigenfunctions necessary for determining the temperature profile are obtained by summation of the first 60 terms in the infinite series of the Kummer function. It can be seen that, due to the jump at the wall, the level of temperature reduction along the tube centerline decreases with increasing rarefaction. Note also that the Maxwell model and the Langmuir model yield almost the same temperature profile, even though, due to the numerical error associated with the lowest order treatment of the term $\frac{\theta_0}{1-\theta_0}\frac{d\theta(r=0,z)}{dz}$ in Eq. (26), the profile of the Langmuir model near the tube inlet (small z^+) deviates from the Maxwell model.

Finally, from the results presented in Figs. 1–4 it can be concluded that both models predict that the Reynolds analogy is preserved in low speed slip flow. In our opinion, the case with $\bar{\sigma} > 1$ is more relevant physically since a large difference in momentum and energy coefficients is extreme rather than typical in the Maxwell model. In addition, by recalling that the reduction of drag coefficient in slip flow is directly related to the decrease of the tangential velocity gradient near the wall due to the velocity slip, one can expect that the same mechanism associated with the temperature jump is responsible for the reduction of heat transfer in slip flow, implying the preservation of the Reynolds analogy in slip-flow regimes. An experimental validation study will be required to clarify this critical issue in the future.

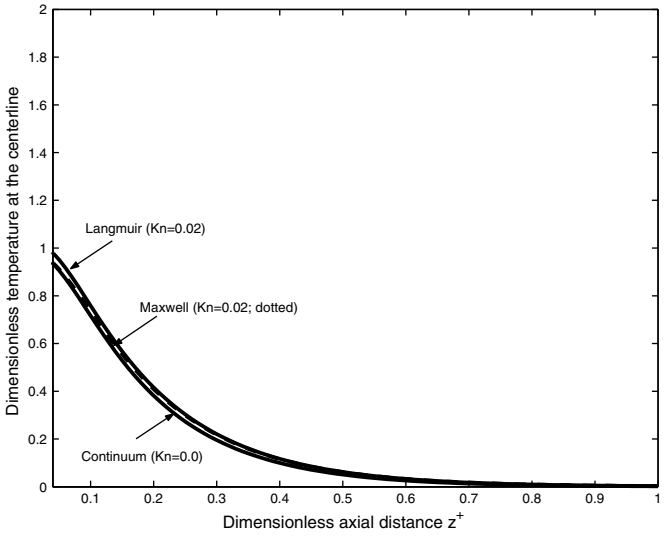

Fig. 4. Comparison of temperature variation at the centerline of the tube. (Langmuir and Maxwell models; $Pe = 10.0, \gamma = \frac{5}{3}, Pr = \frac{2}{3}, \bar{\sigma} = 15/8$).

4. Conclusions

As a step towards answering a fundamental physical question in microscale heat transfer, convective heat transfer in a microtube in slip-flow regimes was investigated using a mathematical method extended from the classical Graetz problem. The slip corrections were made by employing a new Langmuir model based on the concept of adsorption of gases onto solids, as well as the conventional Maxwell model. The effects of axial heat conduction were included by extending a finite integral transform technique to the slip-flow case. We found that the Langmuir model always predicts the reduction of heat transfer with increasing gas rarefaction, and the Maxwell model predicts the same, except when the value of the energy accommodation is much smaller than that of the momentum accommodation. This implies that, for most physical applications, the Reynolds analogy between heat transfer and momentum transfer is preserved in slip-flow regimes with low Mach numbers.

Acknowledgements

We thank the UK's Leverhulme Trust (Research Project Grant No. F/07040/G) and the Engineering and Physical Sciences Research Council (Grant No. GR/S77196/01) for supporting this research financially. We also thank the referees of this paper for their valuable and very helpful comments. R.S.M. thanks the Department of Mechanical Engineering, University of Strathclyde, UK, for the hospitality extended to him during his stay. R.S.M. also wishes to acknowledge the support from the Korea Science and Engineering Foundation (Grant No. R01-2003-000-11735-0).

References

[1] E.B. Arkilic, M.A. Schmidt, K.S. Breuer, Gaseous slip flow in long microchannels, J. Microelectromech. Syst. 6 (2) (1997) 167–178.
[2] J.M. Reese, M.A. Gallis, D.A. Lockerby, New directions in fluid dynamics: non-equilibrium aerodynamic and microsystem flows, Phil. Trans. Roy. Soc. Lond. A 361 (2003) 2967–2988.
[3] S. Chapman, T.G. Cowling, The Mathematical Theory of Non-uniform Gases, third ed., Cambridge University Press, Cambridge, 1970.
[4] G.A. Bird, Molecular Gas Dynamics and the Direct Simulation of Gas Flows, Clarendon Press, Oxford, England, 1994.
[5] B.C. Eu, Kinetic Theory and Irreversible Thermodynamics, John Wiley & Sons Inc., New York, 1992.
[6] R.S. Myong, Thermodynamically consistent hydrodynamic computational models for high-Knudsen-number gas flows, Physics of Fluids 11 (9) (1999) 2788–2802.
[7] R.F. Barron, X. Wang, T.A. Ameel, R.O. Warrington, The Graetz problem extended to slip-flow, Int. J. Heat Mass Transfer 40 (8) (1997) 1817–1823.

[8] F.E. Larrodé, C. Housiadas, Y. Drossinos, Slip-flow heat transfer in circular tubes, Int. J. Heat Mass Transfer 43 (2000) 2669–2680.
[9] M.D. Mikhailov, R.M. Cotta, Mixed symbolic–numerical computation of convective heat transfer with slip flow in microchannels, Int. Commun. Heat Mass Transfer 32 (3–4) (2005) 341–348.
[10] N.G. Hadjiconstantinou, O. Simek, Constant-wall-temperature Nusselt number in micro and nanochannels, Trans. ASME 124 (2002) 356–364.
[11] F. Yan, B. Farouk, Computations of low pressure fluid flow and heat transfer in ducts using the direct simulation monte carlo method, J. Heat Transfer 124 (2002) 609–616.
[12] M.D. Mikhailov, R.M. Cotta, Eigenvalues for the Graetz problem in slip-flow, Int. Commun. Heat Mass Transfer 24 (3) (1997) 449–451.
[13] R.A. Millikan, The general law of fall of a small spherical body through a gas, and its bearing upon the nature of molecular reflection from surfaces, Phys. Rev. 22 (1) (1923) 1–23.
[14] B.C. Eu, R.E. Khayat, G.D. Billing, C. Nyeland, Non-linear transport coefficients and plane couette flow of a viscous, heat-conducting gas between two plates at different temperatures, Can. J. Phys. 65 (1987) 1090–1103.
[15] R.S. Myong, Velocity-slip effect in low-speed microscale gas flows, AIAA Paper No. (2001) 2001–3076.
[16] R.S. Myong, Gaseous slip model based on the Langmuir adsorption isotherm, Phys. Fluids 16 (1) (2004) 104–117.
[17] R.S. Myong, J.M. Reese, R.W. Barber, D.R. Emerson, Velocity slip in microscale cylindrical couette flow: the Langmuir model, Phys. Fluids 17 (2005) 087105.
[18] H.L. Choi, D. Lee, J.S. Maeng, Computation of slip flow in microchannels using Langmuir slip condition, Numer. Heat Transfer Part A—Appl. 44 (1) (2003) 59–71.
[19] I. Langmuir, Surface chemistry, Chem. Rev. 13 (1933) 147.
[20] A.W. Adamson, Physical Chemistry of Surfaces, John Wiley & Sons, New York, 1982.
[21] T.I. Gombosi, Gaskinetic Theory, Cambridge University Press, Cambridge, 2002.
[22] S. Yu, T.A. Ameel, Slip-flow heat transfer in rectangular microchannels, Int. J. Heat Mass Transfer 44 (2001) 4225–4234.
[23] L.C. Burmeister, Convective Heat Transfer, John Wiley & Sons, New York, 1993.
[24] L. Graetz, Uber die Warmeleitungsfahigheit von Flussigkeiten, Annalen der Physik und Chemie 18 (1883) 79–94, Part 1;
L. Graetz, Uber die Warmeleitungsfahigheit von Flussigkeiten, Annalen der Physik und Chemie 25 (1885) 337–357, Part 2.
[25] J.R. Sellars, M. Tribus, J.S. Klein, Heat transfer to laminar flow in a round tube or flat conduit-the Graetz problem extended, Trans. ASME 78 (1956) 441–448.
[26] N.N. Lebedev, Special Functions and their Applications, Dover Pub, New York, 1972.
[27] M. Abramowitz, C.A. Stegun, Handbook of Mathematical Functions with Formulas, Graphs, and Mathematical Tables, Dover Pub, New York, 1972.
[28] M.D. Mikhailov, M.N. Özisik, Unified Analysis and Solutions of Heat and Diffusion, John Wiley & Sons, New York, 1984.
[29] L.J. Slater, Confluent Hypergeometric Functions, Cambridge University Press, Cambridge, 1960.
[30] Y. Bayazitoğlu, M.N. Özisik, On the solution of Graetz type problems with axial conduction, Int. J. Heat Mass Transfer 23 (1980) 1399–1402.
[31] R.M. Cotta, Integral Transforms in Computational Heat and Transfer, CRC Press, Boca Raton, 1993.
[32] C.C. Grosjean, S. Pahor, J. Strnad, Heat transfer in laminar flow through a gap, Appl. Sci. Res. 11 (1963) 292–294.
[33] S. Pahor, J. Strnad, A note on heat transfer in laminar flow through a gap, Appl. Sci. Res. 10 (1961) 81–84.
[34] S.N. Singh, Heat transfer by laminar flow in a cylindrical tube, Appl. Sci. Res. 7 (1957–58) 325–340.
[35] J.C. Maxwell, On stresses in rarefied gases arising from inequalities of temperature, Phil. Trans. Roy. Soc. London 170 (1879) 231.
[36] M. von Smoluchowski, Uber den Temperauresprung bei Warmeleitung in Gasen, Sitzungsberichte Wiene Akademie 107 (1898) 304.
[37] S. Wolfram, The Mathematica Book, Cambridge University Press, Cambridge, 1999.
[38] C. Housiadas, F.E. Larrodé, Y. Drossinos, Numerical Evaluation of the Graetz Series, Int. J. Heat Mass Transfer 42 (1999) 3013–3017.